Heliyon 9 (2023) e19546

Contents lists available at ScienceDirect

Heliyon

journal homepage: www.cell.com/heliyon

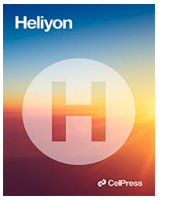

A study related to the treatment of gastric cancer with Xiang-Sha-Liu-Jun-Zi-Tang based on network analysis

Ke Jiang [a,b,c,d], Heli Liu [e], Jie Ge [e], Bo Yang [a,b,c,d], Yu Wang [a,b,c,d], Wenbo Wang [a,b,c,d], Yuqi Wen [a,b,c,d], Siqing Zeng [a,b,c,d], Quan Chen [a,b,c,d], Jun Huang [a,b,c,d], Xingui Xiong [a,b,c,d,*]

[a] *Institute of Integrative Medicine, Department of Integrated Traditional Chinese and Western Medicine, Xiangya Hospital, Central South University, Changsha, 410008, PR China*
[b] *NATCM Key Laboratory of TCM Gan, Xiangya Hospital, Central South University, Changsha, 410008, PR China*
[c] *Hunan Key Laboratory of TCM Gan, Xiangya Hospital, Central South University, Changsha, 410008, PR China*
[d] *National Clinical Research Center for Geriatric Disorders, Xiangya Hospital, Central South University, Changsha, Hunan, 410008, PR China*
[e] *Department of Gastrointestinal Surgery, Xiangya Hospital, Central South University, Changsha, 410008, PR China*

ARTICLE INFO

Keywords:
XSLJZT
GC
Network Pharmacology
Molecular Docking
WGCNA
Mechanism of action

ABSTRACT

Purpose: Xiang-Sha-Liu-Jun-Zi-Tang(XSLJZT) is a common formula for the treatment of Gastric Cancer(GC) and is widely used in clinical practice, however, there is a lack of investigation into its mechanism.

Methods: We collected and organized drug and disease targets, constructed the "XSLJZT-Active Ingredient-Target" visualization network, and performed GO and KEGG functional enrichment analysis of crossover genes, followed by molecular docking of active ingredients and core targets. The best docked monomers were combined with weighted gene co-expression network analysis (WGCNA) and macroscopically analyzed by GO and KEGG enrichment techniques. The results of cluster gene difference analysis, ROC evaluation, and CIBERSORT immune infiltration analysis were evaluated and finally supported by cellular experiments.

Results: The main components of XSLJZT are quercetin, stigmasterol, and naringenin, effectively treat GC by targeting STAT3, TP53 and MAPK3, which are involved in IL-17, TNF and HIF-1 signaling pathways. The results of molecular docking showed that quercetin bound better to the core targets. We performed an in-depth analysis of this monomer and found that quercetin acts on the core targets of TP53, MMP9, TIMP1 and MYC, and is involved in two key signaling pathways, TNF and IL-17, thus effectively treating GC. The experimental results are consistent with our analysis that quercetin inhibits the proliferation of GC cells and promotes apoptosis, and TP53, MYC and TIMP1 are the quercetin targets for the treatment of GC.

Conclusion: The present study tentatively suggests that quercetin, the main active ingredient in XSLJZT, can exert a therapeutic effect on GC by targeting TIMP1.

* Corresponding author. Institute of Integrative Medicine, Department of Integrated Traditional Chinese and Western Medicine, Xiangya Hospital, Central South University, Changsha, 410008, PR China.
E-mail address: xiongxg07@csu.edu.cn (X. Xiong).

https://doi.org/10.1016/j.heliyon.2023.e19546
Received 17 April 2023; Received in revised form 22 August 2023; Accepted 25 August 2023
Available online 28 August 2023

1. Introduction

Gastric cancer (GC) is a globally important disease, the fifth most frequently diagnosed malignancy, and the third most common cause of cancer-related death [1]. Commonly used treatments include surgery, radiotherapy, chemotherapy, and targeted therapy, etc. [2]. Because of their characteristic disease onset, patients are mostly diagnosed by examination after showing obvious symptoms, at which time they are mostly in the middle or late stage, and clinical treatment has been limited [3]. In contrast, Traditional Chinese Medicine (TCM), which is based on a holistic concept and the identification and treatment of symptoms, can improve symptoms and reduce adverse effects to a certain extent. Based on the clinical manifestations of abdominal pain, loss of appetite, weight loss and even hematemesis and melena, GC has been assigned to the categories of " Gastroschisis ", "Stomach regurgitation", and "Choking" in TCM. Among the seven TCM subtypes of GC, the Pi Wei Weakness Type is the most common. Patients with GC are also predisposed to Pi and Wei Qi deficiency during their treatment, which is particularly frequent in patients with advanced GC and those receiving chemotherapy. Therefore, the main treatment for GC today is the method of Jian Pi and Yi Qi.

In recent years, Chinese medicine has shown obvious advantages in the prevention and treatment of GC. XSLJZT, as a basic prescription for the treatment of weakness of the Pi and Wei syndrome, has been widely used in the treatment of digestive system diseases with remarkable efficacy [4–6]. However, few studies have revealed the underlying mechanisms for its treatment of GC. XSLJZT, which emerged from ancient modern medical prescriptions and has been derived from Si-Jun-Zi-Tang(SJZT), is a classic formula for Tonifying the Pi and Qi, Harmonizing the Wei and Dispelling Tan. The medicine prescription consists of eight botanical drugs: Ginseng, Poria cocos, Atractylodes macrocephala, Pinellia ternata, Tangerine peel, Aucklandiae Radix, Villous Amomum Fruit, and licorice. In modern clinical practice, Codonopsis pilosula is often used in place of ginseng. Among them, Codonopsis pilosula is the most important medicine, which can replenish Qi, strengthen Pi, and nourish the Wei. As an auxiliary medicine, Atractylodes macrocephala has the function of invigorating Pi and drying Shi. Then use Poria cocos to promote Shi permeation and tonify the Pi; Pinellia ternate and Tangerine peel are used for resolving Tan and eliminating Shi; Aucklandiae Radix and Villous Amomum Fruit promote Qi circulation to relieve pain. Finally, Licorice plays the role of moderating the property of botanical drugs.

Network pharmacology is based on biological networks to systematically, holistically elucidate the complex interactions between biological systems, drugs, and diseases, and its research features fit with the holistic philosophy of governance in TCM [7,8]. This study also used molecular docking techniques to obtain compounds with therapeutic significance by predicting ligand-target interactions at the molecular level [9], providing a theoretical basis for the treatment of GC with XSLJZT. Then the active ingredients with the lowest binding energy were selected. WGCNA based on the GEO dataset. Through the correlation between the system analysis module and clinical features, the modules closely related to clinical features are obtained, and the core genes related to GC diagnosis are discovered [10]. Finally, it was combined with cellular experiments to verify the therapeutic effect of the effective active ingredients on GC, which also further promoted the study of XSLJZT.

2. Methods

2.1. Acquisition and processing of XSLJZT and GC targets

On the TCMSP (https://old.tcmsp-e.com/tcmsp.php) platform [11], Oral Bioavailability (OB) $\geq$ 30% and Drug Likeness (DL) $\geq$ 0.18 were used as screening conditions. Under this screening condition, we searched the active ingredients and corresponding protein targets of the active ingredients of XSLJZT eight ingredients. Then we converted the screened protein target into the corresponding official gene name through Uniprot database (https://www.uniprot.org/).

We used "gastric cancer" as the key word and used the correlation score $\geq$10.0 as the condition for screening in the GeneCard database (https://www.genecards.org/). Combining the search results from the four databases of Pharm GKB (https://www.pharmgkb.org/), DrugBank (https://www.drugbank.ca/), TTD (https://db.idrblab.net/ttd/), and OMIM (https://www.omim.org/), we eliminated the disease targets that did not intersect. The Venn diagram of XSLJZT and GC targets was drawn using R software. The visualization network of "XSLJZT-Active Ingredient-Target" was constructed in Cytoscape 3.7.2 (http://www.cytoscape.org/).

2.2. Construction of the PPI network with cross-linked genes and enrichment analysis of GO function and KEGG pathway

We introduced the intersection gene mapped by XSLJZT and GC into STRING Database (https://stringdb.org/) [12] and selected "*Homo sapiens*", then set the conditions as "highest confidence" (>0.9), "hide disconnected nodes in the network". The rest were system default parameters. The obtained results were processed by Cytoscape 3.7.2, which allowed us to intuitively display the important target information and the correlation between the two points. The network topology analysis plug-in CytoNCA was used to analyze the topologicasl properties, the colors and sizes of points and edges were adjusted appropriately according to the Degree values. We performed GO function and KEGG pathway enrichment analysis of intersection genes using R software. GO enrichment analysis was performed with the setting $P < 0.05$ and ranked by the number of enriched genes to show the top 20 pathways.

2.3. Molecular Docking

We first downloaded the top nine chemical components of high relevance in 3D.sdf format. They were optimized by chem3D structure and saved in mol2 format. Then we saved the pdb files of the top nine core targets in the RSCB Protein Data Bank (PDB) (http://www.rcsb.org/pdb/) [13]. After that, we used Pymol (http://www.pymol.org/pymol) to remove water and solvent molecules

Table 1
Part of the active ingredient information in XSLJZT.

Number	ID	Chemical name	OB(%)	DL	Source
BZ1	MOL000022	14-acetyl-12-senecioyl-2E,8Z,10E-atractylentriol	63.37	0.3	Atractylodes macrocephala
BZ2	MOL000049	3β-acetoxyatractylone	54.07	0.22	Atractylodes macrocephala
BX6	MOL006957	(3S,6S)-3-(benzyl)-6-(4-hydroxybenzyl)piperazine-2,5-quinone	46.89	0.27	Pinellia ternata
BX8	MOL006967	beta-D-Ribofuranoside, xanthine-9	44.72	0.21	Pinellia ternata
CP2	MOL005815	Citromitin	86.9	0.51	Tangerine peel
CP3	MOL005828	nobiletin	61.67	0.52	Tangerine peel
DS14	MOL002140	Perlolyrine	65.95	0.27	Codonopsis pilosula
DS13	MOL005321	Frutinone A	65.9	0.34	Codonopsis pilosula
FL3	MOL000282	ergosta-7,22E-dien-3beta-ol	43.51	0.72	Poria cocos
FL2	MOL000283	Ergosterol peroxide	40.36	0.81	Poria cocos
GC3	MOL002311	Glycyrol	90.78	0.67	Licorice
GC69	MOL004990	7,2′,4′-trihydroxy - 5-methoxy-3 - arylcoumarin	83.71	0.27	Licorice
MX2	MOL010828	cynaropicrin	67.5	0.38	Aucklandiae Radix
D3	MOL000211	Mairin	55.38	0.78	Aucklandiae Radix
SR4	MOL007536	Stigmasta-5,22-dien-3-beta-yl acetate	46.44	0.86	Villous Amomum Fruit
A1	MOL000449	Stigmasterol	43.83	0.76	Villous Amomum Fruit

Table Note: Only the top 2 OB values for each drug and the active ingredients that act together are listed in the table. OB is the Oral Bioavailability; DL is the Drug Likeness.

Table 2
Chinese medicine repeat ingredient information.

Number	ID	Chemical name	Source
A1	MOL000449	Stigmasterol	Pinellia ternata, Codonopsis pilosula, Aucklandiae Radix, Villous Amomum Fruit
B1	MOL001755	24-Ethylcholest-4-en-3-one	Pinellia ternata, Villous Amomum Fruit
B2	MOL000358	beta-sitosterol	Pinellia ternata, Villous Amomum Fruit
B3	MOL007514	methyl icosa-11,14-dienoate	Codonopsis pilosula, Villous Amomum Fruit
C1	MOL000359	sitosterol	Licorice, Tangerine peel, Aucklandiae Radix
D1	MOL004328	naringenin	Licorice, Tangerine peel
D2	MOL003896	7-Methoxy-2-methyl isoflavone	Licorice, Codonopsis pilosula
D3	MOL000211	Mairin	Licorice, Aucklandiae Radix

as well as add total hydrogen to the core targets. Finally, the results were exported to pdbqt format. The operation of adding full hydrogen to the chemical components was realized by AutoDockTools (https://ccsb.scripps.edu/mgltools/downloads/) [14], and the format was also saved as pdbqt. Finally, we used AutoDock Vina 1.2.3 (https://vina.scripps.edu/) [15,16] to perform docking, the binding energy results of the nine core chemical components docked with each of the nine core targets were obtained. The docking results were partially visualized by Pymol, and the images were saved.

2.4. Acquisition and enrichment analysis of monomeric targets

We first searched the three databases (CTD(http://www.ctdbase.com/), SwissTargetPrediction (http://swisstargetprediction.ch/), Binding DB (https://www.bindingdb.org/)) for the active ingredient with the best docking result obtained in 2.3. Targets with an interaction score greater than 10 in the CTD database were saved and the target name collected in the Binding DB is converted through the STRING database. Finally, DO, GO and KEGG enrichment analyses were performed on the targets obtained after comprehensive removal of duplicates using R software.

2.5. Combining the GEO dataset for GSEA and WGCNA analysis

We selected the GC-related dataset from the GEO database (https://www.ncbi.nlm.nih.gov/geo/), which is closely related to the purpose of the study. The key genes with | logFC |>1 and adjust P.

A GSEA enrichment analysis was obtained to reveal the enrichment situation of differential genes under specific settings. Core genes that play an important role in transcriptional regulation were identified with the help of WGCNA. The best soft threshold (β) was screened in R software using 0.85 as the goodness-of-fit R 2 value, and the genes were grouped according to the (1-TOM). Cluster analysis of the network was carried out by setting the minimum number of genes in the module to 50 and cutting similar modules into one module according to 0.25.

2.6. Construct a new network of the monomer acting on the GC

The genes covered in the module with the highest trait correlation and the genes obtained from the analysis of differences in the data set were taken as intersections for the GC targets to perform enrichment analysis. The interaction between proteins was obtained

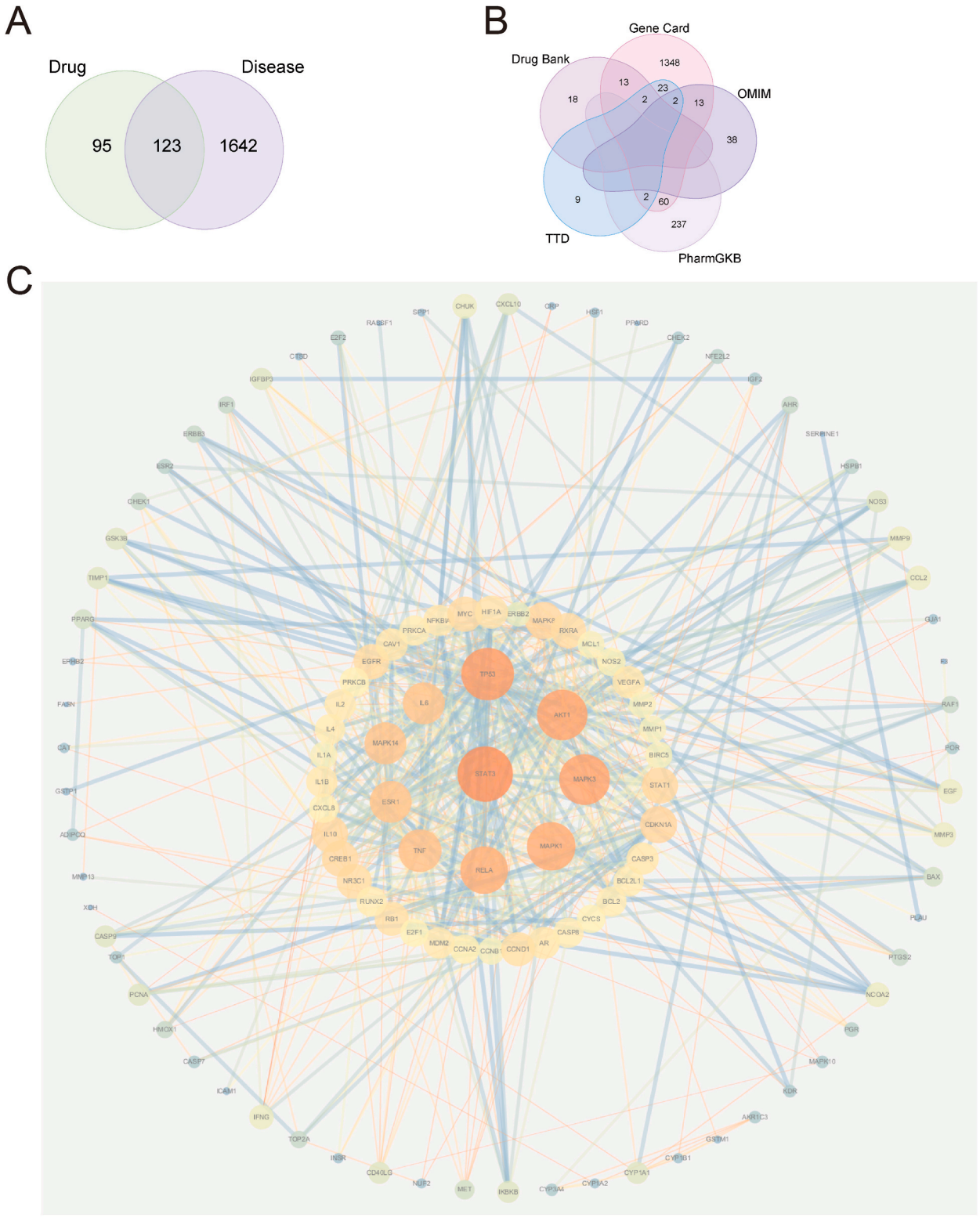

Fig. 1. Target collection and network construction. A) Venn diagram of XSLJZT component targets and GC targets. B) GC-related targets. C) Cytoscape treated PPI network of XSLJZT-treated GC.

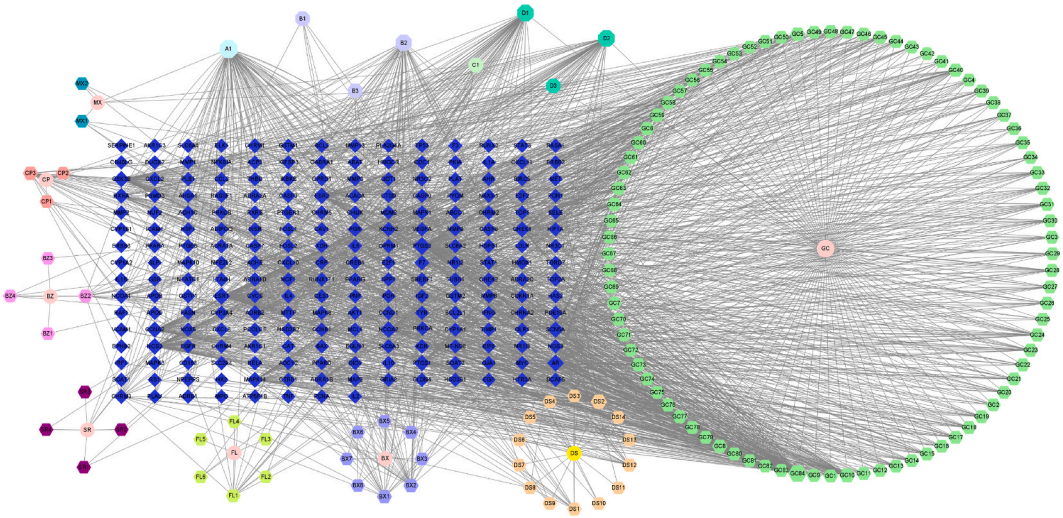

Fig. 2. "XSLJZT-Active Ingredient-Target" visualization network. Note: circle represents drug; square hexagon represents active component; square octagon represents common component information of Chinese medicine; diamond represents target. MX: Aucklandiae Radix; CP: Tangerine peel; BZ: Atractylodes macrocephala; SR: Villous Amomum Fruit; FL: Poria cocos; BX: Pinellia ternata; DS: Codonopsis pilosula; GC: Licorice.

Table 3
Information on the top 10 targets in terms of degree value.

Number	Degree	Name	BetweennessCentrality	ClosenessCentrality
1	39	STAT3	1676.6536	0.5458937
2	36	TP53	1314.4303	0.5255814
3	34	AKT1	1067.682	0.5330189
4	34	MAPK3	777.53485	0.54066986
5	32	MAPK1	661.9699	0.5330189
6	31	RELA	719.2852	0.51834863
7	26	TNF	504.2268	0.47478992
8	25	ESR1	703.24677	0.50446427
9	25	MAPK14	434.82217	0.49561402
10	25	IL6	488.10233	0.46887967

by STRING database. The degree values were calculated using CytoNCA in Cytoscape. Through Mcode plug-in analysis, a core network of drugs with the highest correlation had been built. Then we performed enrichment analysis of genes in the core network.

2.7. Differential analysis of clustered genes, ROC evaluation, and CIBERSORT immune infiltration analysis

The changes in gene expression are significant in the development of GC. The results of the expression matrix normalized by entering the dataset in R software were used to obtain the expression difference maps of genes in the core network by rank sum test. The Receiver Operating Characteristic (ROC) curves were plotted, and the Area Under Curve (AUC) was calculated to evaluate the diagnostic value of the constructed model. We took into account that immune function may be modulated by drugs among different diseases, and therefore calculated the immune infiltration of each sample using the CIBERSOFT algorithm to compare the algorithm results between the two groups. As a reference for developing immunotherapy.

2.8. Experimental verification

2.8.1. Cell culture

MKN-45 cells (purchased from Abiowell, Changsha, China) were cultured in 1640 cell-specific medium (Gibco) containing 10% fetal bovine serum, 100 U/mL penicillin, and 100 U/mL streptomycin, and were cultured in a constant temperature incubator at 37 °C, 5% CO2, and saturated humidity, with fluid changes every 2–3 days, and then digested and passaged when the cells grew to 90% spread.

2.8.2. Cell viability test (CCK-8 assay)

Cells were grouped, and quercetin (purchased from MedChemExpress, China) was added at final concentrations of 0, 20, 40, and 60μmoL/L. After 24 h of incubation, the 96-well plates were removed; the medium was aspirated, and 100 μL of the CCK-8 mixture

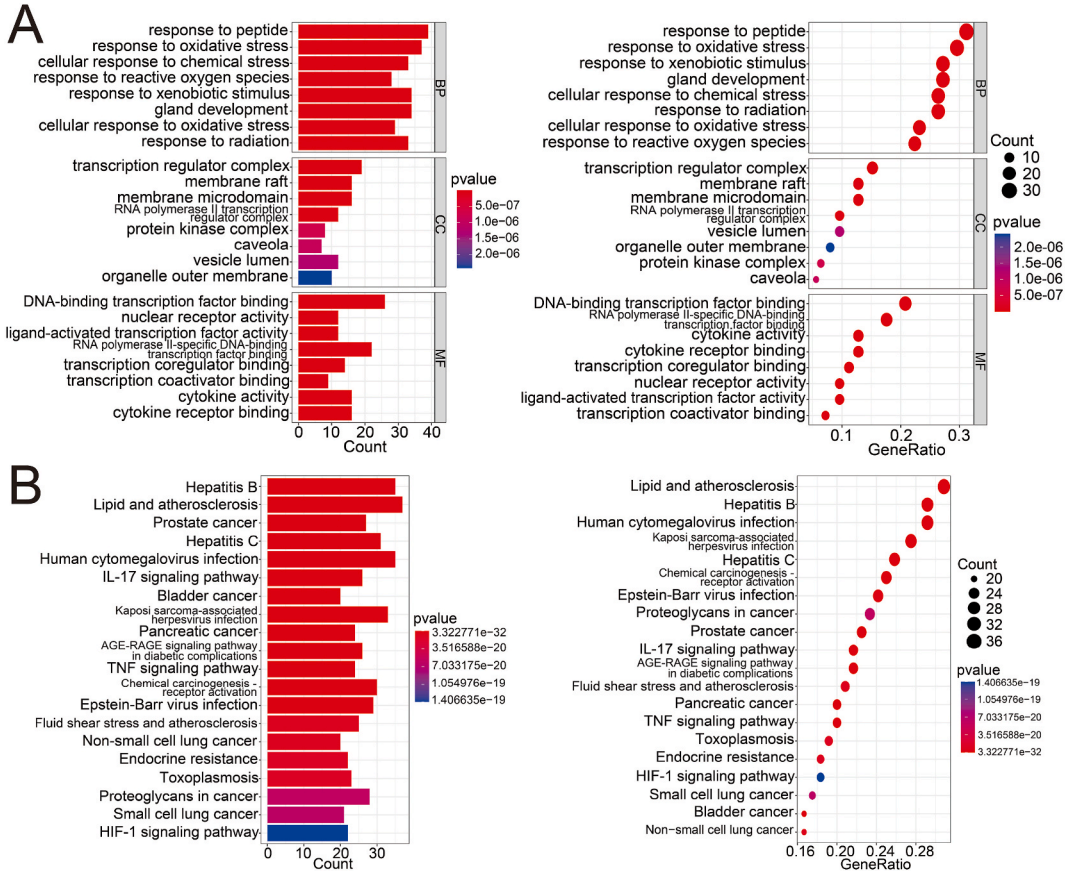

Fig. 3. Enrichment analysis of potential targets of XSLJZT for GC. A) GO. B) KEGG.

Table 4
Molecular docking results of key active ingredients and core targets of XSLJZT (kcal/mol).

Core targets/ chemicals	quercetin	Stigmasterol	naringenin	7-Methoxy-2 methyl isoflavone	beta-sitosterol	luteolin	Kaempferol	baicalein	nobiletin
STAT3	−8.1	−6.1	−7.9	−7.0	−5.9	−7.9	−7.8	−8.2	−7.1
TP53	−7.9	−6.5	−7.5	−6.8	−7.1	−8.1	−7.4	−7.3	−7.1
AKT1	−10.4	−8.5	−9.6	−10.2	−7.2	−10.2	−9.9	−10.2	−8.6
MAPK3	−8.1	−7.9	−8.5	−8.1	−7.1	−8.7	−8.4	−8.5	−7.3
MAPK1	−8.8	−7.5	−8.4	−8.3	−7.1	−8.7	−8.4	−8.4	−7.7
RELA	−9.1	−7.4	−8.9	−6.9	−6.6	−8.4	−9.1	−8.5	−7.2
TNF	−8.1	−7.1	−8.5	−6.9	−7.4	−8.2	−8.2	−8.1	−7.2
ESR1	−8.7	−6.0	−7.7	−6.9	−5.9	−7.4	−8.8	−7.3	−7.6
MAPK14	−9.1	−7.4	−9.1	−9.1	−9.0	−9.3	−8.5	−8.9	−8.4

(CA1210, Solarbio, Beijing, China) was added to each well; the plates were incubated at 37 °C in a 5% CO2 incubator for 2 h; the absorbance value at 450 nm (OD) was measured by an enzyme marker. The whole experiment was repeated three times.

2.8.3. Evaluation of apoptosis by flow cytometry

The cells were inoculated in 6-well plates and incubated at 37 °C in 5% CO2 for 24 h; after adding drugs to the corresponding groups, the incubation was continued for 24 h under the same conditions; the 6-well plates were removed, and the supernatant was collected in centrifuge tubes; 0.5 mL of trypsin digestion was added to each well, and the cells were collected by centrifugation; then the cells were washed by adding pre-chilled PBS and centrifuged. After discarding the supernatant, 400 μL of binding buffer was added to each group; 5 μL of Annexin V-FITC was added and protected from light for 15 min; finally, 10 μL of PI staining solution was added and protected from light for 5 min; the assay was performed on the machine. Each group of experiments was repeated three times.

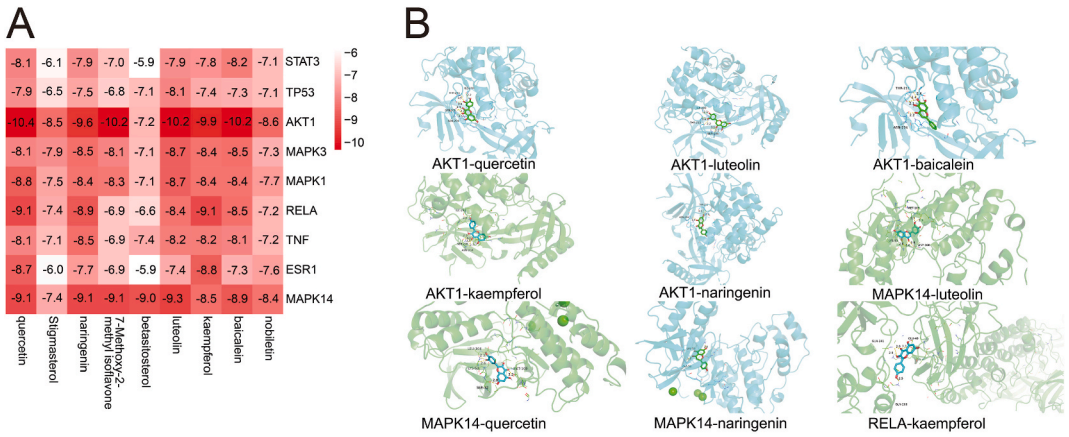

Fig. 4. Molecular docking results presentation. A) Heat map of molecular docking values of XSLJZT key active ingredients and core targets. B) Partial docking model and site map of XSLJZT key active ingredients and core targets.

2.8.4. The expression levels of TP53, TIMP1 and MYC mRNA were detected by qPCR

Total RNA was extracted from cells using an RNA extraction kit (R1200, Solarbio, Beijing, China). Then reverse transcription reactions were performed by removing residual genomic DNA and then adding Hifair® III SuperMix Plus (Yeasen, Shanghai, China) to prepare a reaction system for reverse transcription into cDNA. Finally, Hieff® qPCR SYBR Green Master Mix (Yeasen, Shanghai, China) was used to perform real-time fluorescence quantitative PCR reactions. The experiments were repeated three times. Relative gene expression was calculated using the 2-ΔΔCT method. The Ct value of the target gene was normalized with the Ct value of the internal reference gene (GAPDH), and the primer sequences used were as follows: GAPDH：F—5′- TCAAGAAGGTGGTGAAGCAGG-3’，R—5′-GCGTCAAAGGTGGAGGAGTG-3’; TP53：F— 5′-CTGCCTTCCGGGTCACTG-3’，R—5′-CTCTGGCATTCTGGGAGCTT-3’; TIMP1：F—5′- TGGCTTCTGGCATCCTGTTGTTG-3’，R—5′-ACGCTGGTATAAGGTGGTCTGGTT-3’; and MYC:F—5′-TCTGAGGAGGAACAA-GAAGATGAGGA-3’，R—5′- GCTGCGTAGTTGTGCTGATGTGT-3’.

2.8.5. Statistical analysis

Use the (-ΔΔCt) value for calculation. Then plot with GraphPad. $P < 0.05$ was considered statistically significant.

3. Results

3.1. Target prediction of XSLJZT for GC

A total of 144 active ingredients of XSLJZT were obtained in the TCMSP database according to the selected criteria. Among them, there were 4 compounds in Atractylodes macrocephala, 11 compounds in Pinellia ternata, 5 compounds in Tangerine peel, 17 compounds in Codonopsis pilosula, 6 compounds in Poria cocos, 88 compounds in Licorice, 5 compounds in Aucklandiae Radix, and 8 compounds in Villous Amomum Fruit. The ingredient information was standardized by Uniprot, and 218 ingredient targets were obtained after de-duplication and deletion of invalidation. The information of some active ingredients was collated, and the common ingredients of Chinese medicines were listed (Tables 1 and 2). Integration of GC targets from five disease databases yielded 1765 (Fig. 1B). The Venn diagram (Fig. 1A) shows that there are 123 potential targets for XSLJZT in GC.

3.2. Core components, target acquisition, and enrichment analysis

There were 359 targets and 1727 edges in the " XSLJZT-Active Ingredient-Target" network constructed by Cytoscape. The results are shown in Fig. 2 according to their Degree values and assigned sizes. The three chemical components that play a major role and rank in the top ten in terms of Degree value are quercetin, stigmasterol, and naringenin; the seven effective targets are PTGS2, ESR1, AR, NCOA2, NOS2, SCN5A, and PTGS1.

The results of the String analysis were imported into Cytoscape, the free points were removed to obtain the network with 123 targets and 591 edges. The key core targets information was obtained with the help of CytoNCA. As shown in Fig. 1C, the targets corresponding to STAT3, TP53, AKT1, MAPK3, MAPK1, RELA, TNF, ESR1, MAPK14, and IL6 are shown in a redder color with a larger proportion; the surrounding edges that act with them are thicker and have a dark blue color. This indicates the high importance of these ten targets and the strong connection between them. The results of the data derived from network analysis (Table 3) also suggest that these genes with larger degree values may be effective targets for the treatment of GC with XSLJZT. In addition, we constructed the respective PPI networks of XSLJZT and GC, imported into Cytoscape, took the intersection of the top 10 target genes with Degree values obtained from the three networks and found that TP53, MAPK3, MAPK1, and AKT1 were the core target genes.

The results of GO enrichment analysis show that the main targets of XSLJZT for GC are on different cellular structures including

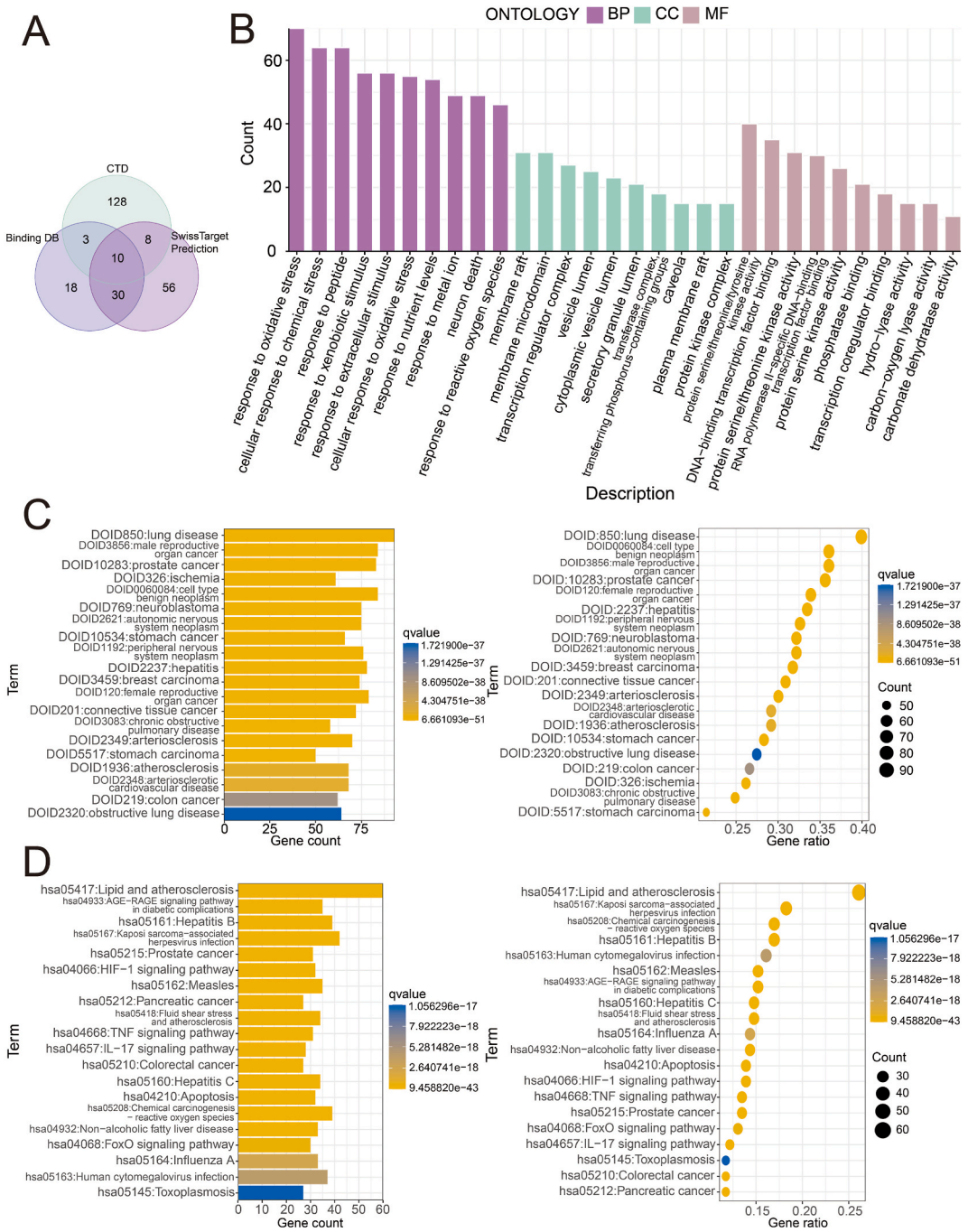

Fig. 5. Collection and enrichment analysis of quercetin targets. A) Venn diagram of quercetin targets in three databases. B) Results of GO enrichment analysis of quercetin targets. C) Results of DO enrichment analysis of quercetin targets. D) Results of KEGG enrichment analysis of quercetin targets.

transcription regulator complex, membrane raft, membrane microdomain, which are involved in diverse biological processes, response to peptide, response to oxidative stress, response to xenobiotic stimulus, etc. Additionally, XSLJZT is enriched for functions such as DNA-binding transcription factor binding, RNA polymerase II-specific DNA-binding transcription factor binding, and cytokine activity. The results of the KEGG pathway enrichment analysis show that the treatment of GC with XSLJZT mainly act on the IL-17 signaling pathway, the TNF signaling pathway, and the HIF-1 signaling pathway (Fig. 3A and B).

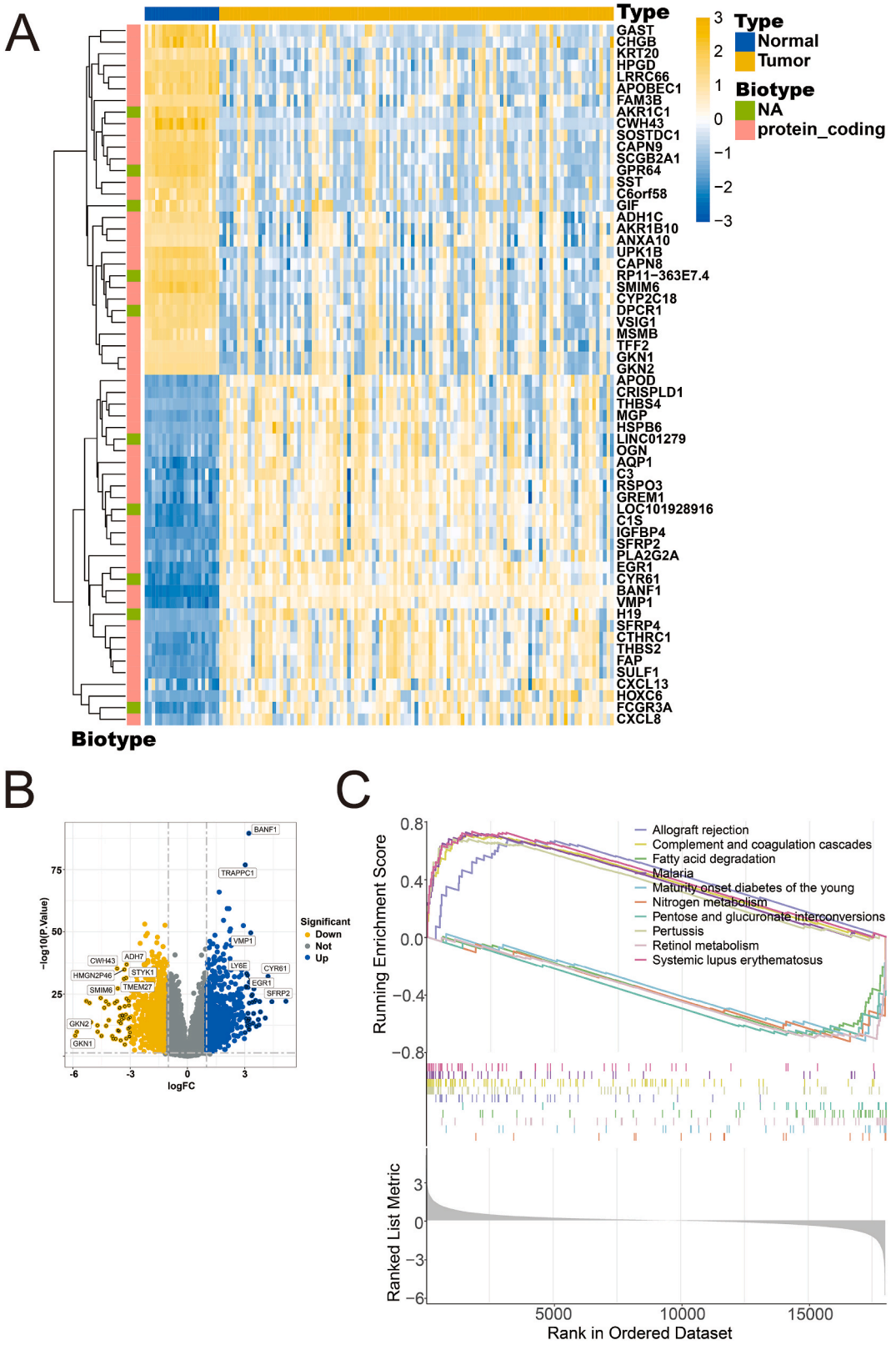

(caption on next page)

Fig. 6. Screening of differentially expressed genes and GESE enrichment analysis. A) Heat map showing the top 30 genes with the largest differences clustered with | logFC | >1 and Adjust P < 0.05. Blue is normal sample, yellow is tumor sample. Blue shows genes with low expression in that sample, yellow is high expression. NA indicates R package temporarily annotated with no results. B) Volcano plot of GC genes under the same conditions, blue represents up-regulated genes in the dataset, yellow represents down-regulated genes, gray refers to no difference genes, and genes with | logFC | >3, P < 0.01 are labeled on the figure annotation. C) GSEA enrichment analysis of GC group and normal group differences the top 5 ranked genes are plotted on the horizontal axis with 0. The five genes on the upper left indicate up-regulated expression and the opposite on the lower right. The gray color shows differential genes, and the horizontal coordinate is the ranking of genes with differential expression between the two groups.

3.3. Results of molecular docking

The top nine chemical components and the top nine core targets were docked by the Autodock Vina module, the binding patterns and affinities between the active components and the core targets were visualized by molecular docking. The minimum binding energies of these nine receptors and ligands were collated to obtain the data shown in Table 4, the results were plotted as a heat map (Fig. 4A). It was found that the binding energies of molecular docking were all ≤ -5.0 kcal/mol, suggesting that the binding ability of the active ingredients to the corresponding targets was good. The lowest total binding energy of −78.3 kcal/mol was obtained by docking quercetin with the core target of XSLJZT. AKT1, MAPK14, MAPK1, and MAPK3 showed the best docking effects with the active ingredients, suggesting the synergistic effect of multiple targets. Finally, some results were visualized for binding energies < -9.0 kcal/mol. The visualized results show that the intermolecular forces are mainly hydrogen bonds (Fig. 4B).

3.4. Acquisition and enrichment analysis of monomeric targets

According to the results of our network drug analysis, quercetin is the monomer with the highest network degree and the lowest total binding energy for docking, with docking results all ≤ -7.0 kcal/mol with each target, like the monomer that plays an important role in the treatment of GC in XSLJZT, however, this monomer is widely found in more than 300 kinds of traditional Chinese medicine, as well as a large number of fruits, vegetables and even many non-medicinal plants. We have pondered whether quercetin is indeed effective in treating GC, and the following is a discussion of its relationship with GC using quercetin as a monomer, in the hope of validating the results of our net drug analysis. We collated the quercetin targets from three databases and combined them with the GEO dataset to verify their clinical value for GC. 253 quercetin targets were obtained by comprehensive weight removal. Then DO, GO, and KEGG enrichment analyses were performed by R software (Fig. 5A–D).

3.5. GSEA and WGCNA analysis based on the GEO dataset

According to the study objectives and conditions, we selected the GSE54129 dataset to obtain gene expression levels and clinical information of GC patients, which is based on the GPL570 platform and contains 21 normal samples and 111 tumor samples. With | logFC | > 1 and adjust P < 0.05, the clustering heat map (Fig. 6A) shows the top 30 genes with the largest differences, among which LINC01279 and SFRP4 are highly expressed in tumor samples and ANXA10 and FAM3B are lowly expressed. Volcano plot (Fig. 6B) shows significant upregulation of gene expressions such as SFRP2 and EGR1, and significant downregulation of gene expressions such as GKN1 and SMIM6. GSEA enrichment analysis demonstrates that in the Tumor group the expression of Allograft rejection, Complement and coagulation cascades, Malaria, Systemic lupus erythematosus are upregulated and expression of Fatty acid degradation, Maturity onset diabetes of the young, Nitrogen metabolism, Pentose and glucuronate interconversions, Retinol metabolism are upregulated in the normal set (Fig. 6C).

The WGCNA analysis filtered out 9 as the optimal soft threshold (Fig. 7A). Hierarchical clustering trees were constructed for all genes, and significant modules were generated (Fig. 7B). Based on these modules, we cut similar modules according to 0.25 to get 18 gene modules. Among them magenta has the highest correlation with GC (R = 0.96, p = 2e-74), followed by the lightcyan module (R = 0.66, p = (4e-18) (Fig. 7C)); and there is also a high correlation between GS and MM in the magenta module (cor = 0.96, p < 1e-200) (Fig. 7D). Fig. 7E and F showed the correlation between gene modules.

3.6. Acquisition of core targets

The disease-PPI network (Fig. 9A) suggests an important role for TP53, MYC in the development of GC. We constructed Venn diagram of quercetin targets and sorted GC genes (Fig. 9B), and contained all these genes into STRING database to construct Network diagram (Fig. 9C). The interprotein interactions between the sorted GC genes and quercetin targets were analyzed by Mcode, and a GC-quercetin core network with the highest correlation was constructed with a score of 7.379, containing 30 points connecting 214 edges. Fig. 9D shows that TP53, MYC, MMP3, MCL1, and CXCL2 are genes common to quercetin and GC.

We analyzed the results of the three enrichments (Fig. 5B–D, Fig. 8A and B, Fig. 10A–C). The results of DO enrichment analysis reveal that GC has a high similarity with the occurrence of such diseases as male reproductive organ cancer, prostate cancer, cell type benigning neoplasm, hepatitis, female reproductive organ cancer and connective tissue cancer. The results of GO enrichment analysis indicate the position that play a major role during treatment are transcription regulator complex and secretory granule lumen. The results of KEGG enrichment show that quercetin is effective in the treatment of GC through two signal pathways, TNF and IL-17. In addition, hepatitis C is also closely related to the occurrence of GC.

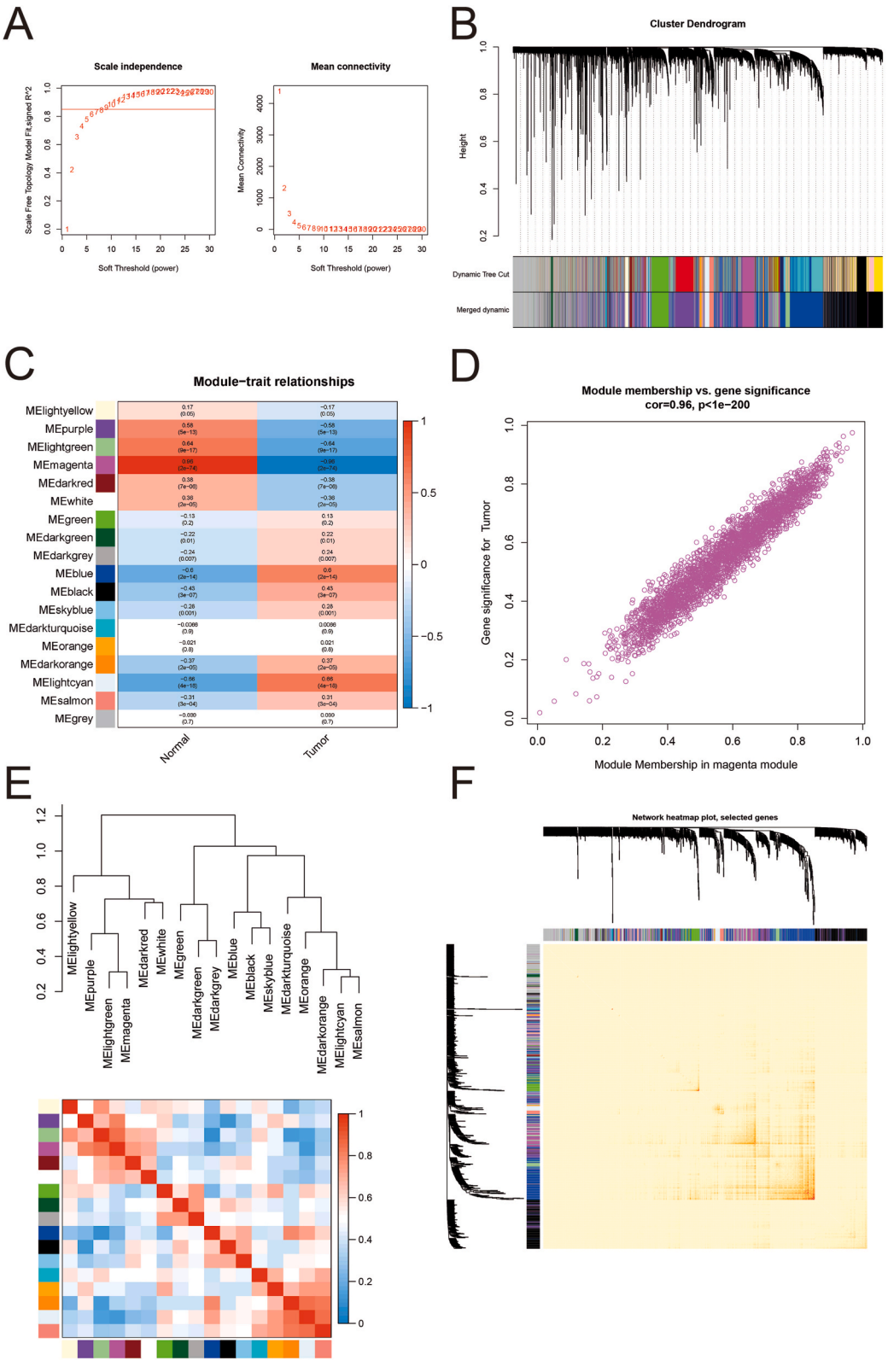

(caption on next page)

Fig. 7. Results of WGCNA. A) Scale-independent, y-axis is the scale-free fit index, x-axis is the soft threshold. B) Dendrogram of GC-related genes based on (1-TOM) clustering; Dynamic Tree Cut shows the original clustering results, Merged dynamic is the result after module merging. C) Heat map of the relationship between module feature genes and clinical features. D) Scatter diagram of magenta module. E, F) Correlation between gene modules.

The top ten genes in the core network were listed according to the Degree values and MCODE scores as in Table 5. The PPI network of quercetin targets, the PPI network of sorted GC genes, and the PPI network of 16 intersecting genes of quercetin and GC, a total of four networks, were then combined for comprehensive analysis. We found that TP53, STAT3, and MAPK1 are the intersecting genes with the core targets of the XSLJZT, suggesting that quercetin is an important component for the action of XSLJZT. TP53 is the target common to all four networks and with the largest degree value, indicating that TP53 may be the core target for the treatment of GC. In addition, the core network obtains MMP9 as the intersection of the top 10 target genes through the four algorithms of MCC, MNC, DMNC and Degree in CytoHubba. Therefore, it is also considered as a significant target. We imported it into String, and the PPI network displays 11 points and 22 edges. Through the visualization operation of Cytoscape, we found that it has high correlation with TGFB1, TIMP1, IL6, LCN2 and other targets(Fig. 10D).

3.7. Differential analysis of cluster genes, ROC evaluation and CIBERSORT immune infiltration analysis

The results of differential analysis (Fig. 11A) show that the expression of TIMP1, MMP9, TP53, CCL2, CXCL2, LIF, MMP3, JUNB, and MYC are significantly upregulated in GC, the expression of CCND1, PRKCD, and CCNB1 are significantly downregulated. The expression levels of CSF2, MAPK1, SMAD3, and SRC are basically unchanged. According to the results of differential expression, we infer that quercetin directly reduces the expression of intersection genes TP53, MYC, MMP3, MCL1, CXCL2; Indirectly regulate the expression of TIMP1 and MMP9, thus achieving the effect of treating GC.

The ROC curves of the genes in the core network were plotted, and all AUCs are found to be > 0.5 (Fig. 11B). TIMP1, MMP2, JUNB, SOCS3, CDK4, MCL1, MYC, and TP53 have high diagnostic value. We note that TIMP1, MMP2, JUNB, SOCS3, CDK4, and the four

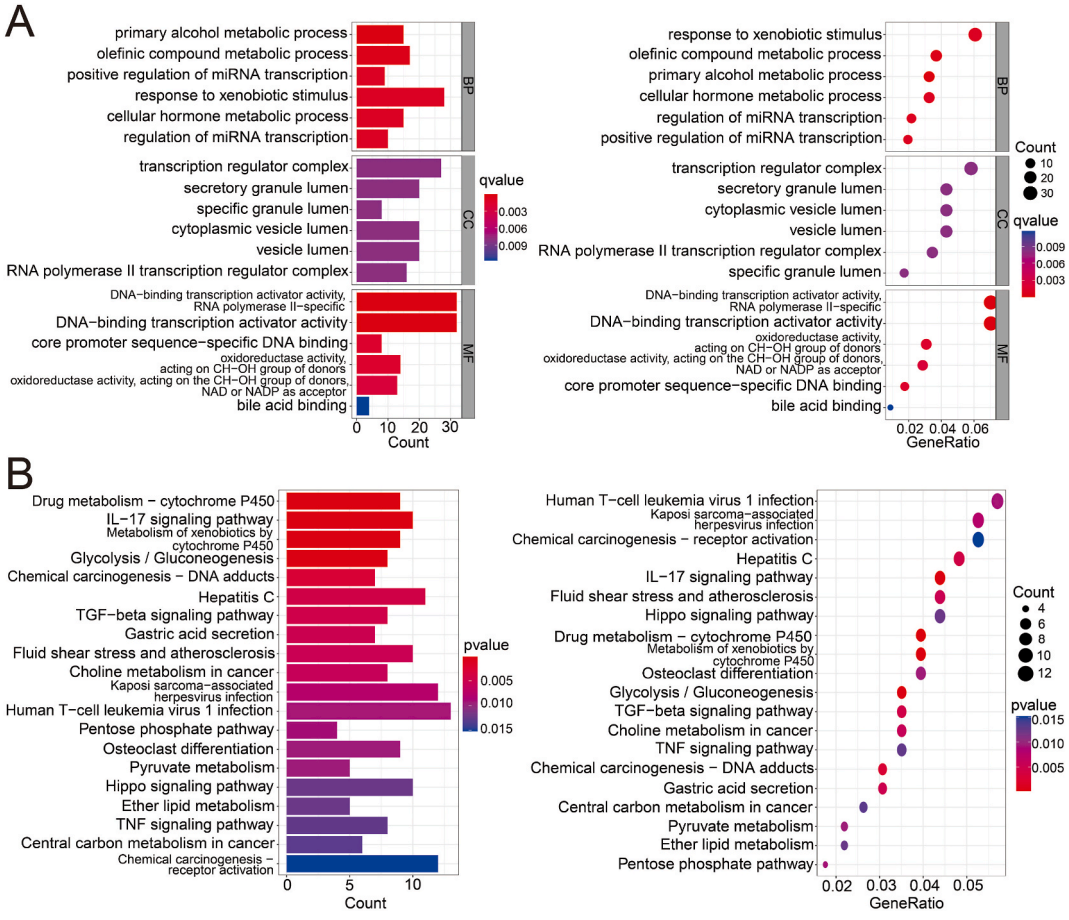

Fig. 8. Use the intersection genes between Magenta module and Dataset differential expression as the sorted GC targets for enrichment analysis. A) GO. B) KEGG.

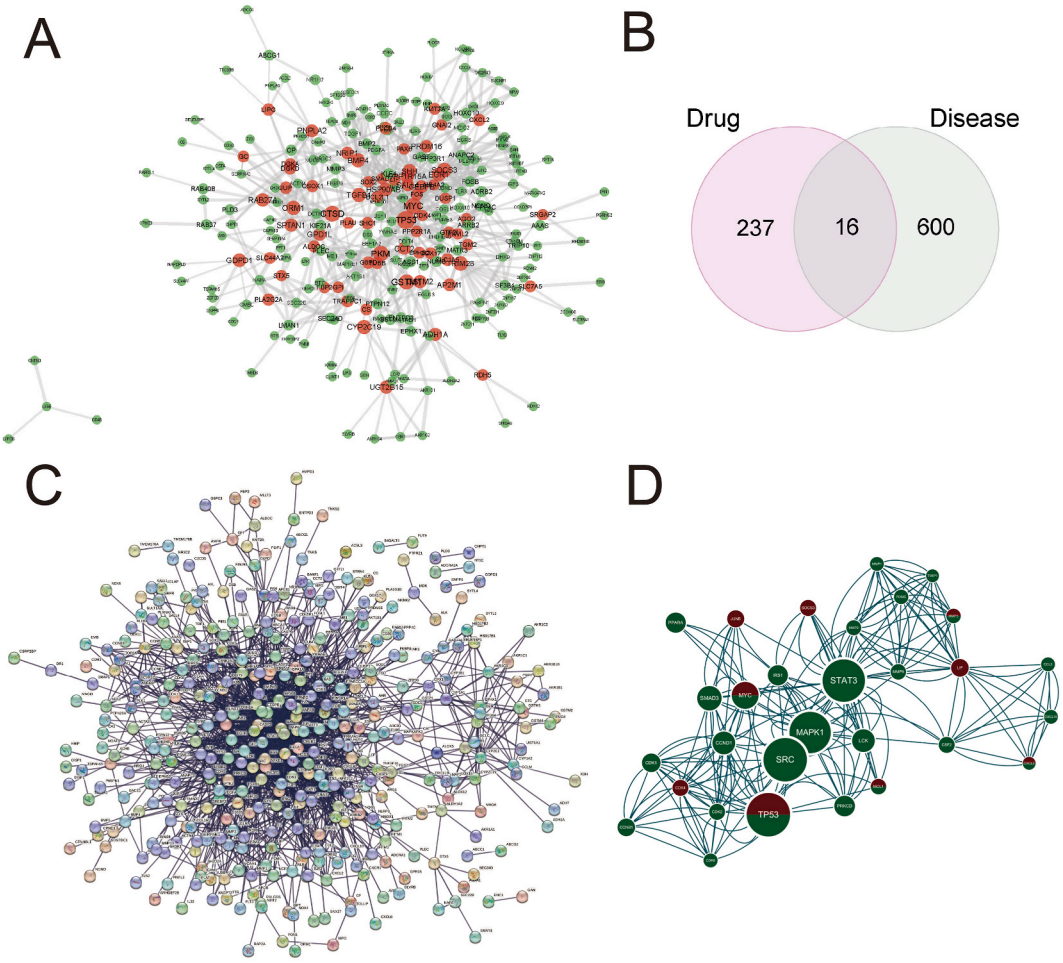

Fig. 9. Construction of core network. A)Remove the free nodes of the sorted GC genes, PPI map of hub genes screened based on betweenness values, with targets greater than the median highlighted in red. B) Venn diagram of quercetin targets and sorted GC genes. C) Network diagram constructed from the STRING database containing all genes for drugs and diseases. D) GC created by Mcode analysis –quercetin core network.

algorithm-derived intersection genes MMP9, which are not disease targets, have higher AUC scores and more significant differential upregulation compare to the normal group. These results indicate that these genes play an important role in the whole network. Quercetin may regulate the activity of the whole network by potentially regulating the expression of these genes, which enriches our understanding of the synergistic treatment of GC with quercetin via multiple targets.

The results of CIBERSORT immune infiltration analysis in Fig. 12 A-C show significantly fewer Plasma cells ($p < 0.001$) and T cells CD4 memory resting ($p < 0.001$). Macrophages M1 ($p < 0.001$) and Macrophages M2 ($p < 0.01$) are significantly higher. Analysis of the relationship between clustered genes and immune infiltration reveal that most genes are negatively correlated with Plasma_cells, T_cells_CD4_memory_resting; and positively correlated with the immune functions of Macrophages_M1, Macrophages_M0 and Neutrophils. The infiltration degree and type of these immune cells may affect the prognosis and treatment response of GC. Therefore, further research on the function and regulatory mechanism of immune cells in GC is expected to provide important insights for the development of more effective GC treatment strategies and immunotherapy. We have known that CD4 T memory resting cells can promote anti-tumor immunity through various mechanisms and regulate the activity of other immune cells. Their infiltration level is negatively correlated with the size of GC tumors [17–19]. M1 and M2 are two different subtypes of macrophages with different functions. M1 macrophages may participate in anti-tumor immune responses by producing inflammatory mediators, whereas M2 macrophages might have immunosuppressive and tumor growth-promoting properties [20,21]. Based on the aforementioned findings, we can reasonably hypothesize that by facilitating the activation of M1 macrophages and increasing the population of CD4 memory resting cells while concurrently inhibiting the presence of M2 macrophages, the anticancer immune response can be enhanced, consequently leading to an improvement in the therapeutic efficacy of GC. We also analyzed role of individual genes in immune infiltration from another perspective, MMP9, CXCL10, and TIMP1 are found to be closely associated with immune cell infiltration.

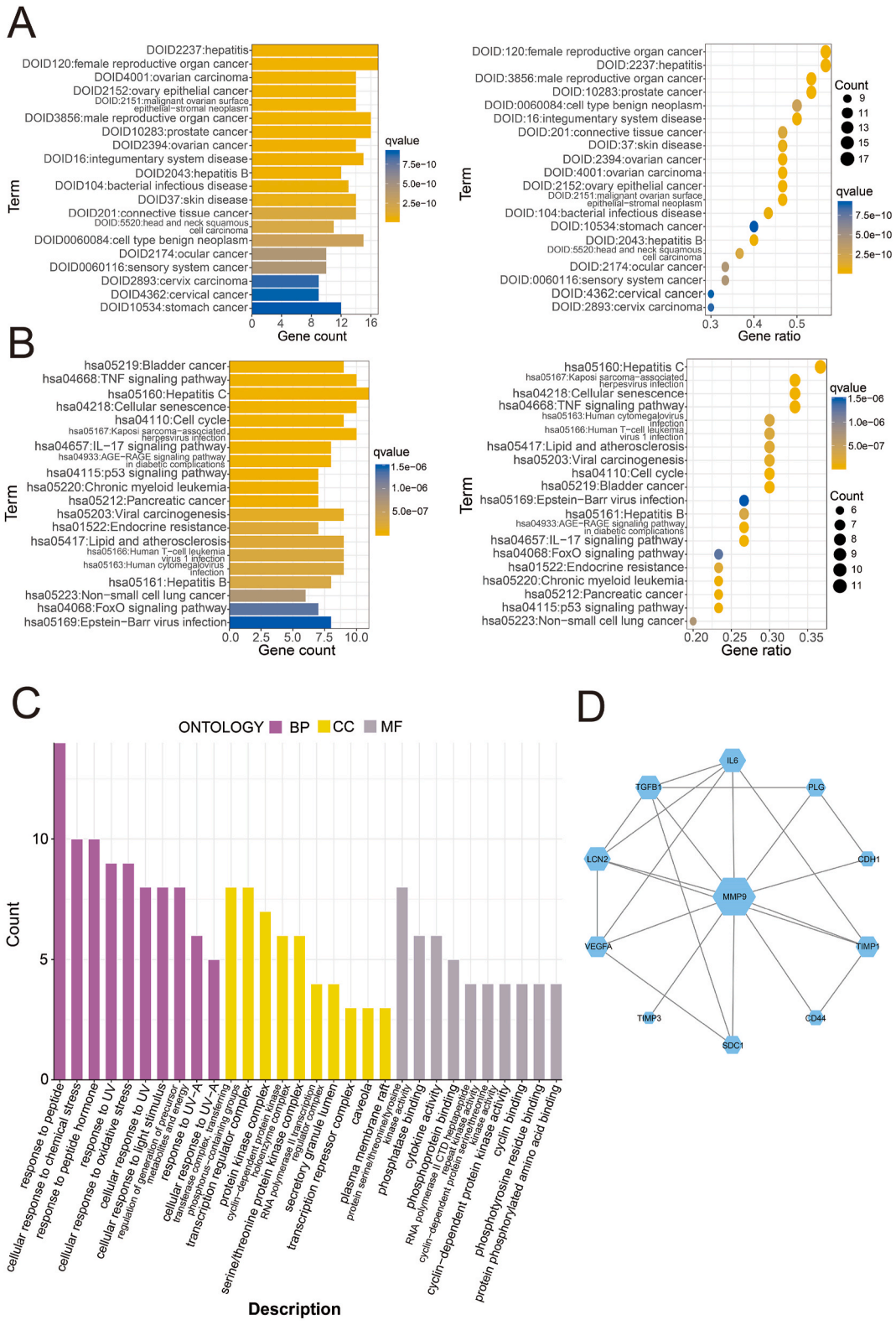

Fig. 10. Core network correlation analysis. A-C) DO, KEGG, GO enrichment analysis of core network genes. D) Correlation analysis on MMP9.

Table 5
Comprehensive analysis of the four networks.

	Drug		Disease		Core Network				16genes	
Number	Name	Degree	Name	Degree	Name	Degree	Name	MCODE Score	Name	Degree
1	TP53	59	TP53	13	TP53	136	CCND1	7.516483516	TP53	4.0
2	STAT3	56	MYC	11	SRC	136	MMP9	7.418181818	FOS	3.0
3	MAPK3	55	FOS	10	STAT3	132	MMP1	7.418181818	MYC	3.0
4	MAPK1	53	EGR1	10	MAPK1	128	LIF	7.418181818	EGR1	3.0
5	SRC	50	SOX2	9	MYC	72	POMC	7.418181818	TGFB1	2.0
6	JUN	49	PPP2R1A	8	SMAD3	62	SRC	7.095238095	CEBPB	2.0
7	EP300	48	JUNB	7	LCK	56	SOCS3	7.000000000	MCL1	2.0
8	RELA	46	PKM	6	CCND1	56	MCL1	7.000000000	BCL2L1	2.0
9	PIK3R1	43	GPI	6	PRKCD	48	CXCL2	7.000000000	MMP3	1.0
10	AKT1	42	BMP4	6	PPARA	46	TIMP1	6.805555556	AKR1C2	1.0

3.8. Analysis of experimental results

The results of CCK8 show that when 20 μM of quercetin was added, the cell viability rate is less than 40%, and the survival rate of GC cells MKN-45 decreases as the concentration of added quercetin increases(Fig. 13A). It indicates that quercetin can inhibit the proliferation of GC cells very well. After using quercetin in the concentration of 20, 40 and 60 μM for the treatment of MKN-45 cell. The results of Annexin V-FITC/PI double staining cell apoptosis detection show that, as the quercetin concentration increases, the apoptosis rate increases as well(Fig. 13B). The results of qPCR show that the expression levels of TIMP1, MYC were lower than the control when 20 μM quercetin was added; the expression levels of TP53, MYC were lower when 40 μM was added; and the expression levels of TP53, TIMP1, MYC were the lowest at 60 μM(Fig. 13C). It indicates that there exists a suitable quercetin concentration around 40 μM, and when the addition concentration is higher than this threshold, the expression levels of the three are lower. Also, the results of qPCR confirm that MYC is a sensitive indicator of quercetin treatment for GC; the effect of TP53 is more obvious at higher concentrations of quercetin addition. In addition, TIMP1 is expected to be a major effective target for quercetin action in GC.

4. Discussion

In this study, we first applied network pharmacology combined with molecular docking to show that XSLJZT is a "multi-component, multi-target, multi-pathway" synergistic agent in the treatment of GC. According to our analysis, the main components of XSLJZT are quercetin, stigmasterol, naringenin, beta-sitosterol, luteolin, and kaempferol. Studies have shown that quercetin can inhibit the proliferation of GC cells, induce apoptosis, regulate the cell cycle, inhibit angiogenesis and metastasis, etc. [22]. Research has shown that stigmasterol can induce apoptosis and protective autophagy by inhibiting the Akt/mTOR pathway in GC cells. The results of the xenograft model indicate that stigmasterol can effectively inhibit the growth of GC tumor [23]. Naringenin can enhance the expression of apoptosis related factors in GC cells, thereby promoting apoptosis of cancer cells. In addition, it can inhibit angiogenesis, inhibit the growth and metastasis of cancer cells, and have a certain preventive effect on tumor occurrence [24]. Beta-sitosterol has been proven to inhibit the malignant proliferation of various tumors (gastric cancer, prostate cancer, colon cancer, etc.) and induce tumor cell apoptosis. Its efficacy, low toxicity, and good safety make it a prospective drug for the treatment of malignant tumors [25]. Besides, In vitro and in vivo studies have shown that luteolin can inhibit GC through a variety of mechanisms, such as regulating Notch, MAPK, PI3K and other signal pathways, inducing G2/M cell cycle arrest and apoptosis [26,27]. Kaempferol, as another active ingredient of XSLJZT, has anti-inflammatory and anti-cancer biological activities. It can inhibit the cell cycle of GC cells, promote autophagy of GC cells. It has therapeutic potential for anti-GC effects [28,29]. In conclusion, the above studies confirm that XSLJZT, as a compound of traditional Chinese medicine, contains major active ingredients that have significant inhibitory effects on GC.

Combining the results of PPI network analysis and molecular docking, the main therapeutic targets of XSLJZT are identified as STAT3, TP53, MAPK3, AKT1, etc. STAT3 is a key signaling molecule and transcription factor for gastric mucosal function, and hyperphosphorylation activation of STAT3 promotes inflammation, cell proliferation, and angiogenesis and inhibits programmed cell death, thereby promoting GC development [30]. TP53 is a common tumor suppressor gene, but it is prone to mutation, and mutant TP53 genes can cause loss of tumor growth inhibition, thus promoting cancer cell proliferation and cell invasion [31]. MAPK3, MAPK1, and MAPK14 all belong to the mitogen-activated protein kinase class of targets. MAPK3 is an important component of the MAPK signaling pathway, which regulates cell growth, adhesion, survival, differentiation and many other biological functions [32]. AKT1 is a serine/threonine-specific protein kinase that plays an important role in the carcinogenesis of GC and is positively correlated with the TNM stage and the depth of infiltration of GC. Interfering with the expression of AKT1 can effectively inhibit the proliferation and migration of GC cells [33,34].

The results of the enrichment analysis reveal that the effective core targets mainly act on the IL-17 signaling pathway, the TNF signaling pathway, and the HIF-1 signaling pathway. IL-17 is a proinflammatory cytokine that plays an important role in the proliferation and progression of GC, and its high expression level is positively correlated with clinical stage and lymph node metastasis [35]. IL17A promotes gastric carcinogenesis through regulation of the IL-17RC/NF-κB/NOX1 pathway [36]. The TNF pathway is involving in cell growth, proliferation, inflammation and immunity. TNF is a tumor therapeutic factor that activates NF-κB signaling and plays a

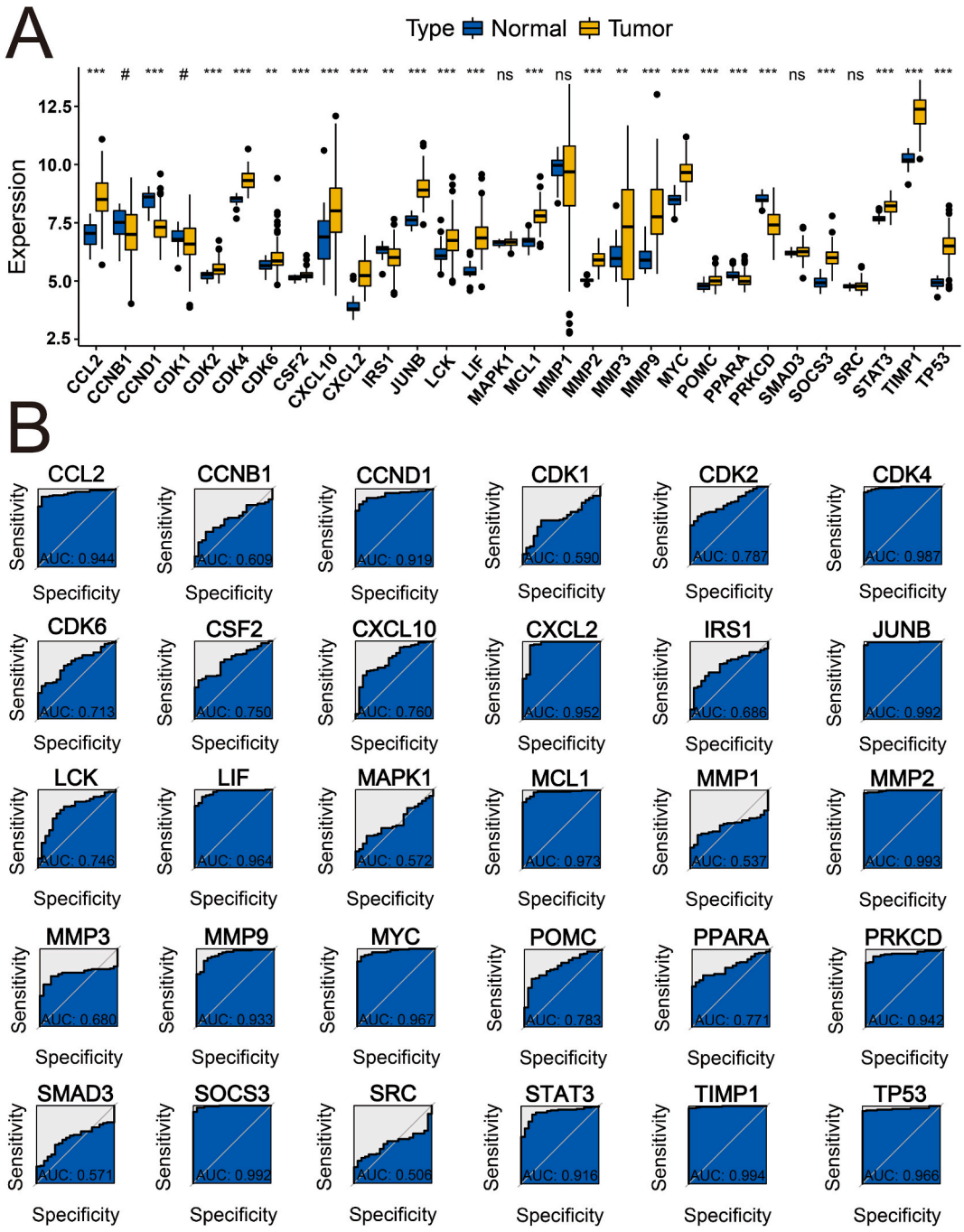

Fig. 11. Variance analysis and ROC evaluation. A) Differential expression of core network genes between normal and tumor groups. B) ROC curve demonstrating the diagnostic value of core network genes for GC.

role in the progression of cancer. Combining with the analysis of the above key targets, it is not difficult to find that TNF plays an indispensable role in the treatment of GC with XSLJZT [37]. The HIF signaling pathway, which accelerates the progression of GC by regulating several genes that affect the proliferation, metastasis, apoptosis, and angiogenesis of GC cells. Among them, HIF-1α enhances GC invasion and metastasis through the induction of EMT. And HIF-1α is not only a possible mediator of gastric carcinogenesis but also correlates with GC severity and poor prognosis [38,39].

Quercetin is present within a variety of herbal medicines and is often a core component of net drug analysis of different compounded prescriptions. In addition to being able to inhibit the proliferation of GC cells through multiple pathways and in multiple ways during in vitro studies. In vivo studies, Lei et al. confirmed that compared with the irinotecan-only groups, the groups with the

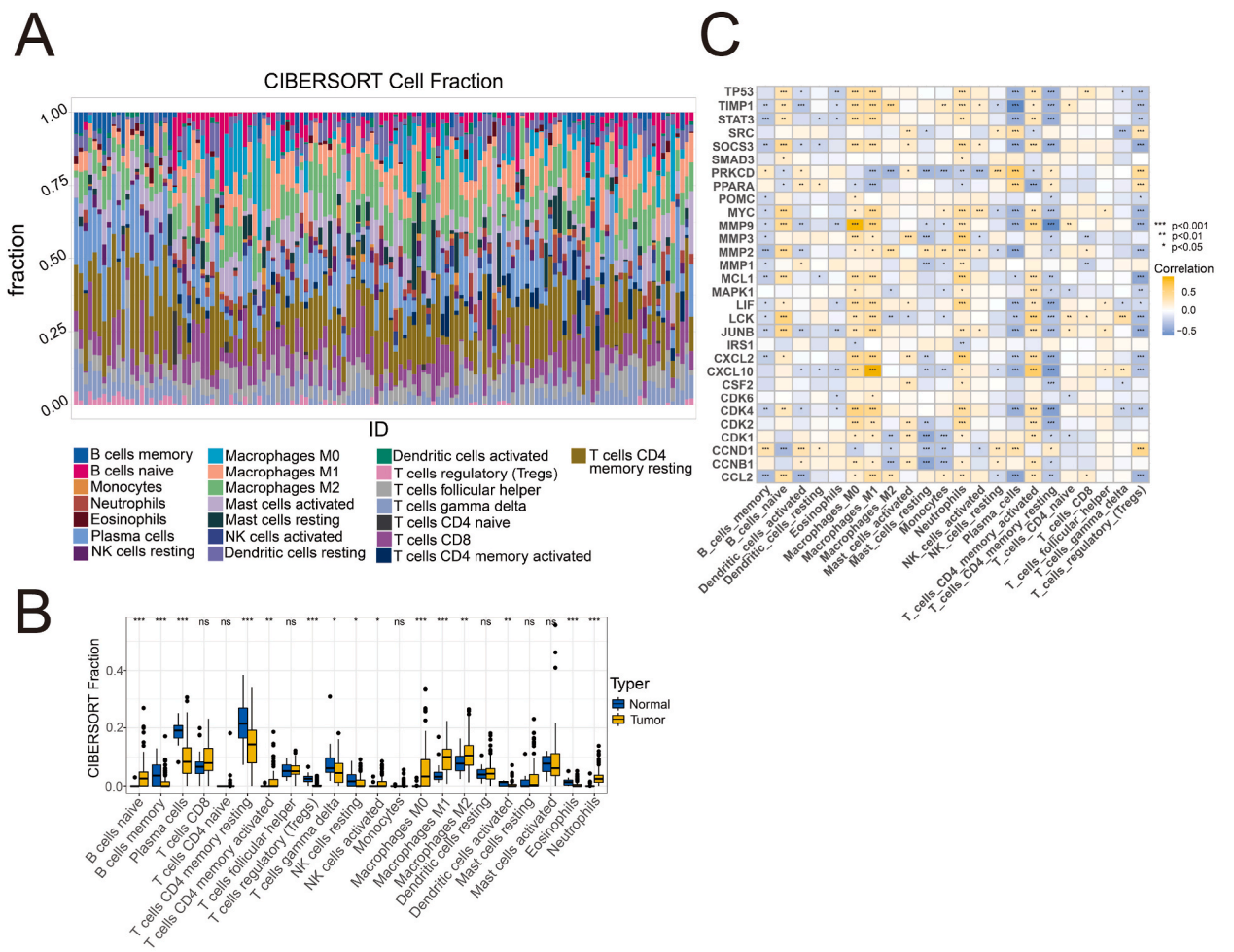

Fig. 12. CIBERSORT immune infiltration analysis on core network genes. A, B) Results of immune infiltration analysis. C) Heat map of correlation between core network genes and immune infiltrating cell function.

combination of irinotecan and quercetin had lower levels of metastasis-related factors and less expression of the COX-2 gene in GC tissues. This indicates that quercetin combined with low-dose antitumor drugs has a better effect on inhibiting GC progression. Lee et al. assessed the anti-cancer effects of quercetin and isoliquiritigenin using in vivo xenograft animals implanted with EBV(+) or EBV (−) human gastric carcinoma. The results indicated that quercetin may be an ideal anticancer agent for the treatment of EBV-related human GC. In addition to its therapeutic role in GC, quercetin has also been found to inhibit the progression of breast cancer, pancreatic cancer, hepatocellular carcinoma, and other cancers. These studies demonstrate that quercetin may prevent the development of tumors [40–44]. Therefore, we selected quercetin, a monomer, to validate the above network pharmacology combined with molecular docking results as well as to further explore the therapeutic mechanism of this monomer in GC. Combining the GSE54129 dataset for WGCNA and other analysis reveal that quercetin is indeed seems to be an important component of XSLJZT for the treatment of GC. The GC-quercetin core network demonstrates that its common genes are TP53, MYC, MMP3, MCL1, and CXCL2, where TP53 is the PPI network of this network with the PPI network of quercetin targets, the PPI network of sorted GC genes and the PPI network of 16 intersecting genes of quercetin and GC, a total of four networks of intersecting genes. Moreover, TP53 exhibits the maximum degree value among all four networks, indicating that TP53 may be the central and core target of quercetin's function.

The results obtained by differential analysis and ROC evaluation of MYC which is the key genes in the core network were also clearly. We know that Myc can participate in the regulation of cell cycle, and its family of proteins includes c-Myc, n-Myc and l-Myc, among which c-Myc plays a role in cell proliferation, apoptosis [45,46], and presumably MYC is also a major target for therapy. It has been reported in the literature that TIMP1 is a biomarker for the diagnosis of GC and that TIMP1 can promote tumor invasion and metastasis, with higher levels associated with poorer prognosis [47,48]. We integrated the core network via the four algorithms in cytoHubba to derive a high correlation between the intersection gene MMP9 and TIMP1; differential analysis yields TIMP1 as the most significantly upregulated gene expressed in GC, with an AUC value of 0.994 for TIMP1, indicating its high diagnostic value; in combination with the results of CIBERSORT immune infiltration analysis TIMP1 is closely associated with immune cell infiltration. TIMP1 is also found to be an important target. Considering the limitation of selecting only one module with the highest correlation for

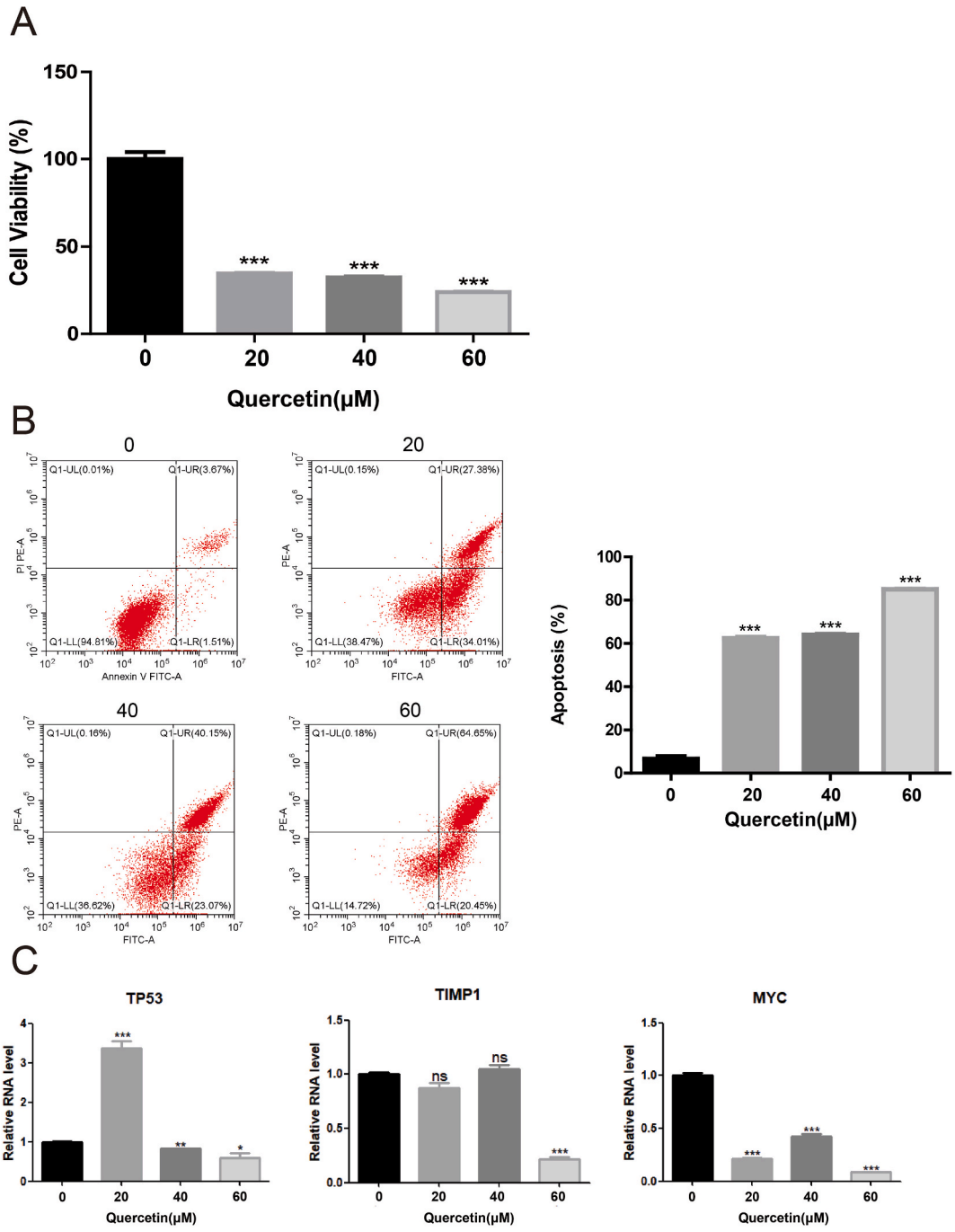

Fig. 13. Experimental results of the effect of quercetin on MKN-45 cells (The levels of significance were set at *$p < 0.05$,**$p < 0.01$ and ***$p < 0.001$.). A) Effect of different concentrations of quercetin on the activity of MKN-45 cells. B) Effects of different concentrations of quercetin on apoptosis of MKN-45 cells. C) qPCR was performed to detect the expression levels of TP53, TIMP1 and MYC mRNA at different concentrations.

core network construction, we reviewed the differentially expressed genes obtained after GC dataset processing and found that TIMP1 is a common target of quercetin and GC, therefore, it is reasonable to infer that TIMP1 in quercetin is a target for the treatment of GC. In the previous analysis, TP53 and MYC are the common targets that act in quercetin. TP53 is commonly used in the treatment of lung, colorectal and pancreatic cancers, and MYC is also used in the treatment of breast cancer. However, studies on the effects of these two targets in quercetin are mostly at the stage of network pharmacology analysis, so we conducted experiments to verify their functions in order to observe their effects more visually. The results of the next cellular assay confirmed our speculation. Quercetin can inhibit the proliferation of GC cells, promote their apoptosis, and exert therapeutic effects on GC by decreasing the expression of TP53, MYC and TIMP1.

The results of three enrichment analyses of quercetin targets, sorted GC genes, and GC–quercetin core network genes, from the perspectives of the function of quercetin, the cause of GC occurrence and the key function of quercetin in regulating GC, it reveals that TNF signaling pathway and IL-17 signaling pathway are the most important pathways involved in the treatment process, which is also consistent with the pathway enrichment results of XSLJZT in treating GC, which laterally confirms that quercetin may be one of the main active components of XSLJZT.

5. Limitation

This study still has some limitations. First, our methods for identifying therapeutic targets are network pharmacology and molecular docking, which rely on the known database and target Protein structure. Therefore, our research is limited by the accuracy and timeliness of the database and the comprehensiveness of compound inclusion. Second, in this study, Quercetin is identified as the most important active ingredient in the treatment of GC. However, the synergistic effects of other active ingredients in XSLJZT in the treatment of GC still need to be further explored, which provides us with ideas for future work.

6. Conclusion

This study reveals that XSLJZT mainly by three active ingredients including quercetin, stigmasterol, and naringenin; targets STAT3, TP53, MAPK3, AKT1 and regulates IL-17 signaling pathway, TNF signaling pathway and HIF-1 signaling pathway to play a synergistic role in the treatment of GC. The active ingredient quercetin was selected for validation and in-depth investigation and the pathway of its enrichment analysis was found to be consistent with XSLJZT, which are also the TNF signaling pathway and the IL-17 signaling pathway. We also experimentally verified that TP53 and MYC are effective targets for its action. In addition, we point out for the first time that TIMP1 may be a potent target for quercetin in the treatment of GC.

Availability of data and materials

The datasets generated and analyzed during the current study are available in the GEO repository [https://www.ncbi.nlm.nih.gov/geo/].

Funding

This project is funded by the Key Project of Hunan Province Traditional Chinese Medicine Research Program (Project number: C2022024).

Author contribution statement

Xingui Xiong; Ke Jiang: Conceived and designed the experiments; Performed the experiments;Analyzed and interpreted the data; Contributed reagents, materials, analysis tools or data; Wrote the paper.Heli Liu; Jie Ge; Bo Yang; Yu Wang; Wenbo Wang; Jun Huang: Conceived and designed the experiments; Analyzed and interpreted the data; Contributed reagents, materials, analysis tools or data; Wrote the paper. Yuqi Wen; Siqing Zeng; Quan Chen: Performed the experiments; Analyzed and interpreted the data.

Data availability statement

Data included in article/supp. Material/referenced in article.

Declaration of competing interest

The authors declare that they have no known competing financial interests or personal relationships that could have appeared to influence the work reported in this paper.

Acknowledgements

Not applicable.

References

[1] F. Bray, et al., Global cancer statistics 2018: GLOBOCAN estimates of incidence and mortality worldwide for 36 cancers in 185 countries, CA A Cancer J. Clin. 68 (6) (2018) 394–424, https://doi.org/10.3322/caac.21492.
[2] E.C. Smyth, et al., Gastric cancer, Lancet 396 (10251) (2020) 635–648, https://doi.org/10.1016/S0140-6736(20)31288-5.
[3] W.L. Guan, Y. He, R.H. Xu, Gastric cancer treatment: recent progress and future perspectives, J. Hematol. Oncol. 16 (1) (2023) 57, https://doi.org/10.1186/s13045-023-01451-3.
[4] Yi-Sing Shih, et al., The effect of Xiang-Sha-Liu-Jun-Zi tang (XSLJZT) on irritable bowel syndrome: a randomized, double-blind, placebo-controlled trial, J. Ethnopharmacol. 238 (2019), 111889, https://doi.org/10.1016/j.jep.2019.111889.
[5] A.M. Kapelemera, et al., Pharmacokinetic herb-drug interactions of Xiang-Sha-Liu-Jun-Zi-Tang and paclitaxel in male sprague dawley rats and its influence on enzyme kinetics in human liver microsomes, Front. Pharmacol. 13 (2022), 858007, https://doi.org/10.3389/fphar.2022.858007.
[6] P. Yue, et al., The efficacy and safety of Xiangsha Liujunzi decoction in the treatment of chronic non-atrophic gastritis: a protocol for a systematic review and meta-analysis, Medicine 100 (4) (2021), e24504, https://doi.org/10.1097/MD.0000000000024504.
[7] C. Nogales, et al., Network pharmacology: curing causal mechanisms instead of treating symptoms, Trends Pharmacol 43 (2) (2022) 136–150, https://doi.org/10.1016/j.tips.2021.11.004.
[8] X. Wang, et al., TCM network pharmacology: a new trend towards combining computational, experimental and clinical approaches, Chin. J. Nat. Med. 19 (1) (2021) 1–11, https://doi.org/10.1016/S1875-5364(21)60001-8.
[9] L. Pinzi, G. Rastelli, Molecular docking: shifting paradigms in drug discovery, Int. J. Mol. Sci. 20 (18) (2019) 4331, https://doi.org/10.3390/ijms20184331.
[10] W. Zhou, et al., Integrated bioinformatics analysis to decipher molecular mechanism of compound Kushen injection for esophageal cancer by combining WGCNA with network pharmacology, Sci. Rep. 10 (1) (2020), 12745, https://doi.org/10.1038/s41598-020-69708-2.
[11] J.L. Ru, et al., TCMSP: a database of systems pharmacology for drug discovery from herbal medicines, J. Cheminf. 6 (2014) 13, https://doi.org/10.1186/1758-2946-6-13.
[12] D. Szklarczyk, et al., The STRING database in 2021: customizable protein-protein networks, and functional characterization of user-uploaded gene/measurement sets, Nucleic Acids Res. 49 (D1) (2021) D605–D612, https://doi.org/10.1093/nar/gkaa1074.
[13] H.R. Drew, et al., Structure of a B-DNA dodecamer: conformation and dynamics 78 (4) (1981) 2179–2183, https://doi.org/10.1073/pnas.78.4.2179.
[14] Y.Q. Zhang, M.F. Sanner, AutoDock CrankPep: combining folding and docking to predict protein-peptide complexes, Bioinformatics 35 (24) (2019) 5121–5127, https://doi.org/10.1093/bioinformatics/btz459.
[15] J. Eberhardt, et al., AutoDock Vina 1.2.0: new docking methods, expanded force field, and Python bindings, J. Chem. Inf. Model. 61 (8) (2021) 3891–3898, https://doi.org/10.1021/acs.jcim.1c00203.
[16] O. Trott, A.J. Olson, AutoDock Vina, Improving the speed and accuracy of docking with a new scoring function, efficient optimization, and multithreading, J. Comput. Chem. 31 (2) (2010) 455–461, https://doi.org/10.1002/jcc.21334.
[17] J. Borst, et al., CD4+ T cell help in cancer immunology and immunotherapy, Nat. Rev. Immunol. 18 (10) (2018) 635–647, https://doi.org/10.1038/s41577-018-0044-0.
[18] M. Melssen, C.L. Slingluff Jr., Vaccines targeting helper T cells for cancer immunotherapy, Curr. Opin. Immunol. 47 (2017) 85–92, https://doi.org/10.1016/j.coi.2017.07.004.
[19] F.X. Li, et al., CD4/CD8 + T cells, DC subsets, Foxp3, and Ido expression are predictive indictors of gastric cancer prognosis, Cancer Med. 8 (17) (2019) 7330–7344, https://doi.org/10.1002/cam4.2596.
[20] V. Gambardella, et al., The role of tumor-associated macrophages in gastric cancer development and their potential as a therapeutic target, Cancer Treat Rev. 86 (2020), 102015, https://doi.org/10.1016/j.ctrv.2020.102015.
[21] W.J. Ma, et al., Identification of a gene prognostic model of gastric cancer based on analysis of tumor mutation burden, Pathol. Oncol. Res. 27 (2021), 1609852, https://doi.org/10.3389/pore.2021.1609852.
[22] S.M. Tang, et al., Pharmacological basis and new insights of quercetin action in respect to its anti-cancer effects, Biomed. Pharmacother. 121 (2020), 109604, https://doi.org/10.1016/j.biopha.2019.109604.
[23] H.G. Zhang, et al., Stigmasterol simultaneously induces apoptosis and protective autophagy by inhibiting akt/mTOR pathway in gastric cancer cells, Front. Oncol. 11 (2021), 629008, https://doi.org/10.3389/fonc.2021.629008.
[24] M. Motallebi, et al., Naringenin: a potential flavonoid phytochemical for cancer therapy, Life Sci. 305 (2022), 120752, https://doi.org/10.1016/j.lfs.2022.120752.
[25] Z. Khan, et al., Multifunctional roles and pharmacological potential of β-sitosterol: emerging evidence toward clinical applications, Chem. Biol. Interact. 365 (2022), 110117, https://doi.org/10.1016/j.cbi.2022.110117.
[26] X.Y. Hao, et al., Antitumor effect of luteolin proven by patient-derived organoids of gastric cancer [published online ahead of print, 2023 Jul 19], Phytother Res. (2023) 1–13, https://doi.org/10.1002/ptr.7963.
[27] M. Çetinkaya, Y. Baran, Therapeutic potential of luteolin on cancer, Vaccines 11 (3) (2023) 554, https://doi.org/10.3390/vaccines11030554.
[28] T.W. Kim, et al., Kaempferol induces autophagic cell death via IRE1-JNK-CHOP pathway and inhibition of G9a in gastric cancer cells, Cell Death Dis. 9 (9) (2018) 875, https://doi.org/10.1038/s41419-018-0930-1.
[29] I. Radziejewska, et al., p-Coumaric acid, kaempferol, astragalin and tiliroside influence the expression of glycoforms in AGS gastric cancer cells, Int. J. Mol. Sci. 23 (15) (2022) 8602, https://doi.org/10.3390/ijms23158602.
[30] M. Ashrafizadeh, et al., Noncoding RNAs as Regulators of STAT3 Pathway in Gastrointestinal Cancers: Roles in Cancer Progression and Therapeutic Response [published Online Ahead of Print, 2023 Mar 23, Med Res Rev, 2023, https://doi.org/10.1002/med.21950.
[31] B. Fito-Lopez, et al., Prevalence, causes and impact of TP53-loss phenocopying events in human tumors, BMC Biol. 21 (1) (2023) 92, https://doi.org/10.1186/s12915-023-01595-1.
[32] M. Drosten, M. Barbacid, Targeting the MAPK pathway in KRAS-driven tumors, Cancer Cell 37 (4) (2020) 543–550, https://doi.org/10.1016/j.ccell.2020.03.013.
[33] J. Gao, et al., Integrating network pharmacology and experimental verification to explore the pharmacological mechanisms of aloin against gastric cancer, Drug Des. Dev. Ther. 16 (2022) 1947–1961, https://doi.org/10.2147/DDDT.S360790.
[34] X.M. Wan, et al., TASP1 promotes proliferation and migration in gastric cancer via EMT and AKT/P-AKT pathway, J Immunol Res 2021 (2021), 5521325, https://doi.org/10.1155/2021/5521325.
[35] J. Bastid, et al., The emerging role of the IL-17B/IL-17RB pathway in cancer, Front. Immunol. 11 (2020) 718, https://doi.org/10.3389/fimmu.2020.00718.
[36] J.H. Kang, et al., IL-17A promotes Helicobacter pylori-induced gastric carcinogenesis via interactions with IL-17RC, Gastric Cancer 26 (1) (2023) 82–94, https://doi.org/10.1007/s10120-022-01342-5.
[37] Y.Y. Su, et al., Ensemble learning model for identifying the hallmark genes of NFκB/TNF signaling pathway in cancers, J. Transl. Med. 21 (1) (2023) 485, https://doi.org/10.1186/s12967-023-04355-5.
[38] M.Q. Li, et al., HIF in gastric cancer: regulation and therapeutic target, Molecules 27 (15) (2022) 4893, https://doi.org/10.3390/molecules27154893.
[39] Y.N. Huang, et al., Dextran sulfate effects EMT of human gastric cancer cells by reducing HIF-1α/TGF-β, J. Cancer 12 (11) (2021) 3367–3377, https://doi.org/10.7150/jca.55550.
[40] C.S. Lei, et al., Effects of quercetin combined with anticancer drugs on metastasis-associated factors of gastric cancer cells: in vitro and in vivo studies, J. Nutr. Biochem. 51 (2018) 105–113, https://doi.org/10.1016/j.jnutbio.2017.09.011.
[41] H.H. Lee, et al., Anti-cancer effect of quercetin in xenograft models with EBV-associated human gastric carcinoma, Molecules 21 (10) (2016) 1286, https://doi.org/10.3390/molecules21101286.

[42] X.M. Xi, et al., The biphasic effect of flavonoids on oxidative stress and cell proliferation in breast cancer cells, Antioxidants 11 (4) (2022) 622, https://doi.org/10.3390/antiox11040622.
[43] Y.Y. Guo, et al., Quercetin suppresses pancreatic ductal adenocarcinoma progression via inhibition of SHH and TGF-β/Smad signaling pathways, Cell Biol. Toxicol. 37 (3) (2021) 479–496, https://doi.org/10.1007/s10565-020-09562-0.
[44] Y. Ji, et al., Quercetin inhibits growth of hepatocellular carcinoma by apoptosis induction in part via autophagy stimulation in mice, J. Nutr. Biochem. 69 (2019) 108–119, https://doi.org/10.1016/j.jnutbio.2019.03.018.
[45] G. Zhang, et al., HECTD3 promotes gastric cancer progression by mediating the polyubiquitination of c-MYC, Cell Death Dis. 8 (1) (2022) 185, https://doi.org/10.1038/s41420-022-01001-9.
[46] G.S. Barbosa-Jobim, et al., Biflorin inhibits the proliferation of gastric cancer cells by decreasing MYC expression, Toxicol. Vitro 63 (2020), 104735, https://doi.org/10.1016/j.tiv.2019.104735.
[47] Z. Li, et al., The prognostic and diagnostic value of tissue inhibitor of metalloproteinases gene family and potential function in gastric cancer, J. Cancer 12 (13) (2021) 4086–4098, https://doi.org/10.7150/jca.57808.
[48] G. Song, et al., TIMP1 is a prognostic marker for the progression and metastasis of colon cancer through FAK-PI3K/AKT and MAPK pathway, J. Exp. Clin. Cancer Res. 35 (1) (2016) 148, https://doi.org/10.1186/s13046-016-0427-7.